High-quality AlGaN/GaN superlattices for near- and mid-infrared intersubband transitions

C. Bayram[a)]
IBM Research, T. J. Watson Research Center, Yorktown Heights, New York 10598, USA

(Received 29 August 2011; accepted 8 December 2011; published online 6 January 2012)

A pulsed layer-by-layer deposition (PLLD) technique possessing triple growth rates compared to conventional growth techniques is developed by metal−organic chemical vapor deposition to realize high-quality high-aluminum content ordered $Al_XGa_{(1-X)}N$ $(0.5 < X)$. X-ray diffraction, photoluminescence, and transmission measurements are employed to demonstrate control over aluminum content, structural uniformity, and optical quality in the ordered $Al_XGa_{(1-X)}N$. To show the feasibility of device applications, $Al_XGa_{(1-X)}N$ as barrier and GaN as well are employed in superlattices demonstrating intersubband transitions in the infrared regime. Effects of well width and barrier aluminum content on the intersubband absorption characteristics are reported. © *2012 American Institute of Physics*. [doi:10.1063/1.3675468]

I. INTRODUCTION

III-nitrides are composed of AlGaInN compounds and offer direct bandgap along their entire composition. As such, early III-nitride optoelectronics research has explored the various compositions of this material system and resulted in mainstream ultraviolet and visible spectral applications such as water purification and solid state lighting.[1] Recently, ongoing studies point out the significance of gap-engineering in addition to composition-engineering to enable terahertz applications.[2]

Unique material characteristics of III-nitrides such as large conduction-band offset (AlN/GaN ~ 2.1 eV), electron-effective mass ($m^* \sim 0.2 - 0.3 \times m_0$), and longitudinal optical phonon energy (~90 meV) motivate for intersubband (ISB) device applications. AlN and GaN have the lattice mismatch of 2.4%, can be realized crack-free and be grown pseudomorphically.[3] However, III-nitrides are piezoelectric materials. In conventional c-plane growth, these highly strained layers generate multi-MV/cm electric fields.[4] Thus, interface or SL thickness fluctuations degrade the superlattice quality significantly.[4] Another problem is AlN/GaN or GaN/AlN interface stability, and their dependence on (GaN or AlN) templates.[5] Moreover, the embedded GaN layer gets thinner during subsequent AlN growth.[6] Because of these growth challenges, only preliminary devices such as optical modulators and tunnel diodes are realized to date.[7]

Much of these ISB device efforts have been realized by molecular beam epitaxy (MBE)[2,7]— an ultra-low pressure deposition system—mainly because of sharp interface requirements for tens of periods of AlGaN/GaN structures embedded in the ISB devices. On the other hand, metal–organic chemical vapor deposition (MOCVD) is the most economically-feasible technique for the mass-production of such ISB devices and of critical importance for the potential penetration of these emerging devices to our lives—yet ISB devices grown by MOCVD remains almost unexplored.[8] We have recently shown that proper growth techniques can enable such high-quality III-Nitride intersubband devices[9] and further research and development by MOCVD is essential.[10]

In this work, we report on a pulsed layer-by-layer deposition (PLLD) technique possessing triple growth rates compared to conventional growth techniques for the realization of high-quality high-aluminum-content ordered $Al_XGa_{(1-X)}N$ $(0.5 < X)$. Structural and optical characterizations are realized to assess the effect of PLLD schemes on $Al_XGa_{(1-X)}N$ layers. In addition, we show that the PLLD technique is suitable for intersubband device applications via demonstrating ISB absorption in the infrared wavelengths, and report on the effects of aluminum-content in the barrier and well width on ISB absorption characteristics.

II. EXPERIMENT

PLLD of AlGaN was realized in an AIXTRON 200/4-HT horizontal flow low-pressure MOCVD reactor at a temperature of 1035 °C under 50 mbar. Trimethlyaluminum (TMAl) and trimethylgallium (TMGa) are used as the metal-organic precursors for Al and Ga, respectively; ammonia (NH_3) and hydrogen (H_2) are used as the anion source and carrier gas, respectively. Silane (SiH_4) is used as the *n*-type dopant source. All structures are grown on top of high-quality 1-μm-thick AlN epilayer on double-side polished (001) sapphire.

Figure 1(a) shows the growth scheme of PLLD. The PLLD of ordered AlGaN is based on growing AlN and GaN sublayers with controlled thicknesses. The AlN sublayer (step I composed of Phase A and B) is grown by temporal separation of TMAl and NH_3 that prevents parasitic reactions[11] leading to an increased material quality and growth rate. This is followed by GaN sublayer growth (step II) where TMGa and NH_3 are supplied together. In between the sublayers, a surface nitridization (step III) is optional but employed in this work based on the need for interface quality. The flexibility of this approach is that each sublayer (AlN and GaN) growth can be optimized in its own "growth

a)Electronic mail: cbayram@us.ibm.com.

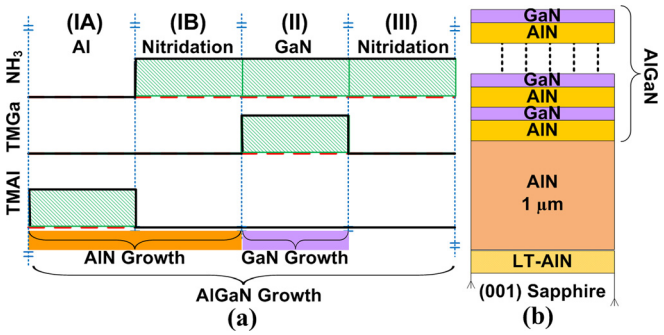

FIG. 1. (Color online) (a) Optimized pulsed layer-by-layer deposition sequence of ordered AlGaN. The technique consists of two main deposition steps: (I) AlN deposition, which is realized via pulsing TMAl and NH_3 to enhance aluminum adatom mobility and growth rate, and (II) conventional GaN deposition, which is realized by supplying TMGa and NH_3 simultaneously. Step III is optional but added as necessary for nitridizing the surface for better interface sharpness in the demonstration of ISB transitions. (b) The ordering of AlN and GaN epilayers in ordered AlGaN as a result of optimized pulsed layer-by-layer deposition sequence is illustrated.

time window" (I for AlN and II for GaN); thus, no significant trade-offs in the reactor conditioning during the AlGaN growth are necessary. This approach increased the material quality as well as tripled the growth rate with respect to conventional growth scheme in which all metal-organics (TMAl, TMGa) and hydrides (NH_3) are supplied together. Ordered AlGaN structure is sketched in Fig. 1(b). To study the effect of the PLLD scheme on structural and optical quality of ordered AlGaN, various timing sequences are studied as listed in Table I.

Table I (samples A through G) summarizes the effect of PLLD growth scheme and of silicon (*n*-type dopant) on the optical quality, structural integrity, and aluminum content of ordered AlGaN. These samples are characterized via photoluminescence (summarized in Table I and seen in Fig. 2), transmission (seen in Fig. 2 inset), and x-ray diffraction (XRD) (summarized in Table I and seen in Fig. 3 inset) measurements. To understand the effect of ordering on AlGaN, bandgap energy (E_g), and aluminum content (X_{Al}) are determined separately from photoluminescence (PL) and XRD measurements and compared. The bandgap energy from PL (E_g^{PL}) was extracted from the spectral measurements by Gaussian fitting. The average aluminum content (X_{Al}^{XRD}) from XRD was calculated from (002) omega/2theta XRD measurements via $X_{Al}^{XRD} = (C_{AlGaN} - C_{GaN}^0)/(C_{AlN}^0 - C_{GaN}^0)$ where C_{GaN}^0 and C_{AlN}^0 are the free-standing lattice parameters of GaN and AlN, and C_{AlGaN} is the average lattice constant of the superlattice (SL) determined from x-ray analysis.[12] The aluminum content from PL (X_{Al}^{PL}) and bandgap energy from XRD (E_g^{XRD}) were calculated via Vegard's law.[13]

III. RESULTS AND ANALYSIS

A. Ordering in PLLD-grown AlGaN

Table I shows that E_g^{XRD} is observed to be larger than E_g^{PL} for all AlGaN samples (sample G is an exception because of the high doping amount and will be discussed later). The tens of meV difference between bandgaps calculated from PL and XRD measurements can be explained through ordering in AlGaN as follows. The Fig. 3 inset shows a representative (002) omega/2theta XRD of an ordered sample C. The ordering within the AlGaN sample C is identified with the first-order fine satellite peaks. This ordering in AlGaN is expected from PLLD as discussed earlier. Because of the ordering, AlGaN peak PL wavelength is observed to redshift with respect to the disordered alloy of the same composition. The bandgap reduction is caused by localization of the band-edge wave functions in the GaN layer. Ordered $Al_XGa_{(1-X)}N$ thus can be seen as a natural quantum well structure where electrons and holes are localized and confined in the monolayer GaN quantum wells.[14] Thus, the significant difference between bandgaps calculated from PL and XRD measurements is a result of the ordering in AlGaN.

Room temperature PL and transmission studies are realized to further investigate the behavior of ordered AlGaN. Figure 2 shows the room temperature photoluminescence of samples A ($Al_{0.94}Ga_{0.06}N$), C ($Al_{0.74}Ga_{0.26}N$), and G ($Al_{0.54}Ga_{0.46}N$). Only one dominant AlGaN PL peak is observed showing the high material quality and uniform ordering in the samples. The Fig. 2 inset shows the room temperature transmission of select samples: AlN template, B, C, D, G, and GaN (grown on AlN template). All samples

TABLE I. Optical and structural characterization summary of the $Al_XGa_{(1-X)}N$ samples labeled from A to G, grown by pulsed-layer-by-layer deposition scheme. Bandgap energy (E_g) and aluminum content (X_{Al}) are determined from both photoluminescence (PL) and x-ray diffraction (XRD) measurements for comparison and superscripted as necessary. XRD FWHM belongs to the 0th-order (002) $Al_XGa_{(1-X)}N$ peak.

	PLLD Scheme									
ID	Si (sccpm)	IA (sec)	IB (sec)	II (sec)	III (sec)	$(X_{Al}^{PL}$ (%)) E_g^{PL} (eV)		X_{Al}^{XRD} (%) (E_g^{XRD} (eV))		XRD FWHM (arcsec)
A	0	4	2	4[a]	2	(90.0)	5.80	93.8	(5.91)	62.1
B	0	4	2	4	2	(50.1)	4.48	61.6	(4.82)	381.0
						(13.5)	3.64	18.5	(3.73)	500<
C	0	4	2	2	2	(68.0)	5.02	74.4	(5.24)	117.0
D	2	4	2	2	2	(71.4)	5.13	78.2	(5.37)	91.2
E	20	4	2	2	2	(68.6)	5.04	80.0	(5.43)	105.0
F	20	2	2	1	2	(75.1)	5.26	79.8	(5.42)	212.0
G	20	2	2	2	2	(53.7)	4.58	53.7	(4.58)	271.0

[a]Refers to the step where no NH_3 was supplied. Underscore refers to where silicon dopant (Si) was introduced.

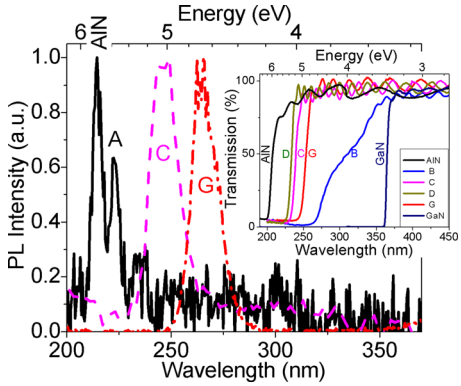

FIG. 2. (Color online) Room temperature photoluminescence of ordered AlGaN samples (A, C, and G) showing the aluminum content tunability. Inset shows the room temperature transmission of AlN, ordered AlGaN samples (B, C, D, and G), and GaN.

except B have clear absorption band-edges showing high-quality ordering. The bandgap energies obtained from transmittance of AlN template, C, D, G, and GaN are determined to be 6.17, 5.20, 5.32, 4.87, and 3.40 eV, respectively. Sample B possesses two AlGaN-related peaks in XRD spectra, as summarized in Table I, and displays non-uniformity in the ordering of AlGaN agreeing with the two absorption features in transmittance. This non-uniformity in sample B will be discussed in the next paragraph.

Density of screw dislocations (D_B) in III-nitrides can be estimated from[12] $D_B = \beta^2/9 \cdot b^2$ where β is FWHM of (0002) peak, and b is the length of the burger vector of screw dislocations. Thus, density of dislocations is proportional with the square of the FWHM. Decreasing FWHM values indicate a lower dislocation density in the material. From Table I, by comparing samples A and B, it is seen that to achieve ordering, the GaN thickness should be thin ($\sim$1 nm) otherwise phase separation occurs in AlGaN (as seen in sample B) leading to multiple aluminum content sublayers (for sample B, two aluminum contents are identified as 61.6% and 18.5%). This is because when GaN is grown under compressive strain (as grown on AlN templates) and is thicker than the critical thickness, the growth mode will change to 3D growth during the nitridization (step 4 of the growth scheme in Table I) and will form GaN quantum dots via the Stranski-Krastanov mode.[15] This is why sample B, which has a thick GaN sublayer ($> \sim 2$ nm), possesses two absorption features in transmittance.

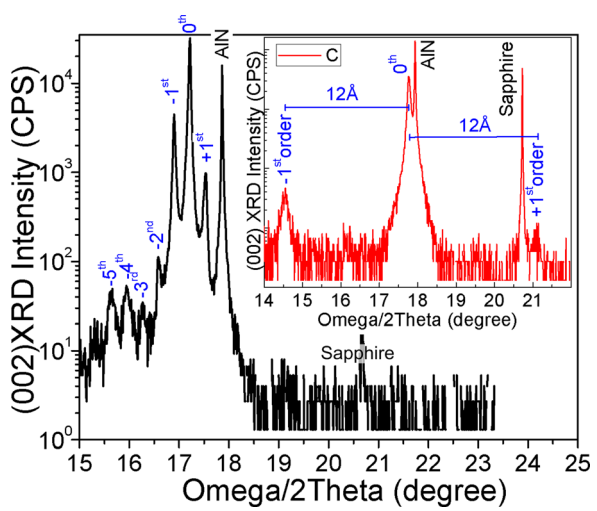

FIG. 3. (Color online) (002) omega/2theta XRD of AlGaN/GaN SLs composed of 2.0-nm-thick ordered $Al_{0.74}Ga_{0.26}N$ (sample ID: C in Table I) and 1.1-nm-thick GaN. The inset shows (002) omega/2theta XRD of ordered $Al_{0.74}Ga_{0.26}N$ (sample ID: C in Table I). The ordering of AlGaN is identified via fine-defined XRD satellite peaks in the inset.

The effect of silicon on ordered AlGaN is deduced by examining the samples C, D, and E, as summarized in Table I. The small addition of silicon improved the ordering (C to D) and decreased the XRD FWHM; however, further silicon flow increase degraded the material quality. This is attributed to the anti-surfactant effects of silicon, which at higher concentrations degrade layer-by-layer growth,[15] hindering the ordering of AlN and GaN by surface roughening.

The effect of GaN and AlN thicknesses on ordered AlGaN is identified by examining the samples E and F. When the growth time for both AlN and GaN layers are halved (decreased from 4 to 2 and 2 to 1 s, respectively), the average aluminum content in AlGaN stayed the same ($\sim 79.9 \pm 0.1\%$) whereas XRD FWHM doubled suggesting decrease in the ordering quality (reduced AlN and GaN interface sharpness). These findings suggest that both AlN (t_{AlN}) and GaN (t_{GaN}) thicknesses are crucial in achieving high-quality ordered AlGaN, and under given growth conditions, our results identify the ideal thickness ranges as $5.4\ \text{Å} < t_{AlN}, t_{GaN} < 10.8\ \text{Å}$ to tune the aluminum content (X) of $53.7\% < X < 93.8\%$ in ordered $Al_XGa_{(1-X)}N$.

In summary, XRD, PL, and transmission studies confirm that by proper adjustment of the MOCVD growth scheme, high-quality ordering in AlGaN can be achieved by PLLD, and high-quality ordered AlGaN demonstrates a single and narrow PL peak, XRD 0th order AlGaN peak (along with higher order satellite peaks), and a clear absorption band-edge. To show that these ordered AlGaN layers are indeed suitable for device applications, we demonstrate intersubband transitions, which are highly sensitive to interfaces and material quality, by employing ordered AlGaN structures in the next section.

B. High-quality AlGaN/GaN superlattices for intersubband transitions

Figure 3 displays the (002) omega/2theta XRD of a 50-period SL composed of 2.0-nm-thick ordered $Al_{0.74}Ga_{0.26}N$ (sample C in Table I) and 10.7-nm-thick GaN. Layer thicknesses are calibrated via independent SL growths. AlGaN 0th order peak and angular separation between satellite peaks are used to extract constituent layer thicknesses. As seen in Fig. 3, ordered AlGaN/GaN SL possesses satellite peaks up to fifth order, which demonstrates the high-quality interface.[12]

To study the effect of aluminum content on ISB measurements, AlGaN/GaN SLs composed of 2.7-nm-thick GaN wells and 3.0-nm-thick $Al_XGa_{(1-X)}N$ barriers with $X = 1.00$, 0.74, and 0.20 were grown. Because of the low aluminum content, $Al_{0.20}Ga_{0.80}N$ barrier was grown conventionally (via simultaneous supply of TMAl, TMGa, and NH_3 into the growth chamber). In addition, another set of SLs composed

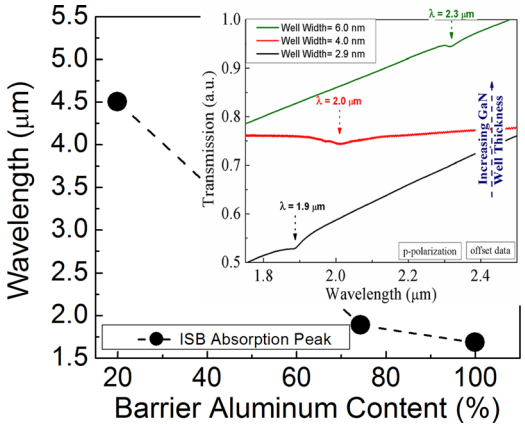

FIG. 4. (Color online) ISB absorption peaks of $Al_XGa_{(1-X)}N$/GaN superlattices as a function of barrier aluminum content and well width. (a) Dependency of ISB absorption peaks on barrier aluminum content. The GaN well width is fixed at 2.7 nm. (b) Dependency of ISB absorption peaks on GaN well thickness. Transmission is plotted as a function of wavelength for three well widths of 2.9, 4.0, and 6.0 nm. For all cases, the barrier is 3.0-nm-thick ordered $Al_{0.74}Ga_{0.26}N$.

of 3.0-nm-thick ordered $Al_{0.74}Ga_{0.26}N$ barriers and various-thickness (2.9, 4.0, and 6.0 nm) GaN wells were grown to study the effect of well width on ISB absorption peak wavelength.

After the MOCVD growths, samples were prepared for ISB absorption measurement via dicing (into 4-mm-long bars) and polishing (45° angle facets are polished on both sides to form a multipass waveguide). The infrared transmission was measured at room temperature using a Fourier transform infrared spectrometer. A wire-grid polarizer was inserted into the beam-path just before the sample to select either p- or s-polarization for the incident light. The difference between the absorption of p- and s-polarized light was used to identify ISB absorption.

Figure 4 plots ISB absorption peaks of $Al_XGa_{(1-X)}N$/GaN superlattices as a function of barrier aluminum content. For the same GaN well width of 2.7 nm, decreasing the barrier aluminum content from 100 to 74, and down to 20% shifts the ISB absorption feature up from 1.56 to 1.89, and up to 4.5 μm. This is because decreasing aluminum content in the barrier leads to decreasing conduction band-offset, which decreases the energy separation of the first two confined states of the well. The Fig. 4 inset displays the (p-polarized) transmission of $Al_XGa_{(1-X)}N$/GaN superlattices as a function of GaN well width for the 3.0-nm-thick ordered $Al_{0.74}Ga_{0.26}N$ barrier. The absorption feature (attributed to transition from first to second electronic state) redshifts with increasing well width. Increasing the well width (from 2.9 to 6.0 nm) redshifts the ISB absorption peak (from 1.89 to 2.32 μm). This is because the two first confined states of the well become closer in energy with increasing well width.

In summary, PLLD by MOCVD is a suitable technique for achieving high-quality ordered AlGaN and can be employed in ISB devices. By tuning the aluminum content in the barrier and controlling the well widths, we have demonstrated ISB absorption in the infrared spectrum.

IV. CONCLUSION

In summary, we introduced PLLD as a reliable MOCVD technique to achieve fast growth rates, high material quality,and uniform ordering in high aluminum content $Al_XGa_{(1-X)}N$ ($0.5 < X$). PLDD-grown AlGaN is ordered as determined from XRD measurements and possesses a single PL peak and absorption edge like a conventional AlGaN. Ordering in AlGaN is shown to lower the bandgap because of quantum confinement effects. The study of ISB absorption samples employing AlN, ordered $Al_{0.74}Ga_{0.26}N$, and $Al_{0.20}Ga_{0.80}N$ as barrier showed that lowering the aluminum content in the barrier or increasing the GaN well width redshift the ISB peak absorption wavelength. High material quality and acute thickness control are shown to be crucial in controlling infrared ISB transitions.

ACKNOWLEDGMENTS

Dr. Bayram acknowledges the support, interest, and encouragement of Professor Manijeh Razeghi (from Northwestern University, IL, USA) and Dr. Devendra Sadana (from IBM Research, T.J. Watson Research Center, NY, USA), and the valuable collaboration with the Center for Quantum Devices of Northwestern University, IL, USA.

[1]H. Morkoc, *Handbook of Nitride Semiconductors and Devices*, Vol. 3 (Wiley, New York, 2008).
[2]M. Razeghi, IEEE Photon. J. **3**, 263 (2011).
[3]A. D. Bykhovski, B. L. Gelmont, and M. S. Shur, J. Appl. Phys. **81**, 6332 (1997).
[4]N. Suzuki, N. Iizuka, and K. Kaneko, Jpn. J. Appl. Phys. **42**, 132 (2002).
[5]C. Adelmann, E. Sarigiannidou, D. Jalabert, Y. Hori, J.-L. Rouviere, B. Daudin, S. Fanget, C. Bru-Chevallier, T. Shibata, and M. Tanaka, Appl. Phys. Lett. **82**, 4154 (2003).
[6]N. Gogneau, D. Jalabert, E. Monroy, E. Sarigiannidou, J. L. Rouviere, T. Shibata, M. Tanaka, J. M. Gerard, and B. Daudin, J. Appl. Phys. **96**, 1104 (2004).
[7]H. Machhadani, P. Kandaswamy, S. Sakr, A. Vardi, A. Wirtmüller, L. Nevou, F. Guillot, G. Pozzovivo, M. Tchernycheva, A. Lupu, L. Vivien, P. Crozat, E. Warde, C. Bougerol, S. Schacham, G. Strasser, G. Bahir, E. Monroy, and F. H. Julien, New J. Phys. **11**, 125023 (2009).
[8]C. Bayram, N. Péré-laperne, R. McClintock, B. Fain, and M. Razeghi, Appl. Phys. Lett. **94**, 121902 (2009).
[9]C. Bayram, Z. Vashaei, and M. Razeghi, Appl. Phys. Lett. **97**, 181109 (2010).
[10]I. Ahmad, B. Krishnan, B. Zhang, Q. Fareed, M. Lachab, J. Dion, and A. Khan, Phys. Status Solidi A **208**, 1501 (2011).
[11]J. P. Zhang, H. M. Wang, W. H. Sun, V. Adivarahan, S. Wu, A. Chitnis, C. Q. Chen, M. Shatalov, E. Kuokstis, J. W. Tang, and M. A. Khan, J. Electron. Mater. **32**, 364 (2003).
[12]M. A. Moram and M. E. Vickers, Rep. Prog. Phys. **72**, 036502 (2009).
[13]M. Androulidaki, N. T. Pelekanos, K. Tsagaraki, E. Dimakis, E. Iliopoulos, A. Adikimenakis, E. Bellet-Amalric, D. Jalabert, and A. Georgakilas, Phys. Status Solidi C **3**, 1866 (2006).
[14]M. Albrecht, L. Lymperakis, J. Neugebauer, J. E. Northrup, L. Kirste, M. Leroux, I. Grzegory, S. Porowski, and H. P. Strunk, Phys. Rev. B **71**, 035314 (2005).
[15]J. C. Zhang, B. Meyler, A. Vardi, G. Bahir, and J. Salzman, J. Appl. Phys. **104**, 044307 (2008).